Metal-to-insulator transition and magnetic ordering in $CaRu_{1-x}Cu_xO_3$

I. M. Bradarić,[1,*] I. Felner,[2] and M. Gospodinov[3]
[1]*Laboratory for Theoretical and Condensed Matter Physics, The "Vinča" Institute of Nuclear Sciences, P.O. Box 522, 11001 Belgrade, Serbia, Yugoslavia*
[2]*The Racah Institute of Physics, The Hebrew University of Jerusalem, Jerusalem 91904, Israel*
[3]*Bulgarian Academy of Sciences, Institute of Solid State Physics, 72 Tzarigradsko Chaussee Boulevard, Sofia 1784, Bulgaria*
(Received 11 November 2000; revised manuscript received 24 May 2001; published 17 December 2001)

$CaRuO_3$ is a perovskite with an orthorhombic distortion, and is believed to be close to magnetic ordering. Magnetic studies of single-crystal and polycrystalline $CaRu_{1-x}Cu_xO_3$ ($0 \leqslant x \leqslant 15$ at. % Cu) reveal that a spin-glass-like transition develops for $x \leqslant 7$ at. % Cu. The obtained value for the effective magnetic moment $p_{\text{eff}} = 3.55\mu_B$ for an $x = 5$ at. % Cu single crystal, indicates the presence of Ru^{5+}. At higher Cu concentrations more complex magnetic behaviors are observed. Electrical resistivity measured on polycrystalline samples shows a metal-to-insulator transition at 51 K for only 2-at. % Cu. Charge compensation, which is assumed to be present upon $Cu^{2+/3+}$ substitution, induces the appearance of Ru^{5+} and/or the creation of oxygen vacancies in a crystal structure. Since the observed changes in physical properties are completely attributable to the charge compensation, they *cannot be related* to behaviors of a pure compound where no such mechanism is present. This study provides the criterion for ''good'' chemical probes for studying Ru-based perovskites.

DOI: 10.1103/PhysRevB.65.024421 PACS number(s): 75.50.Lk, 71.30.+h, 75.30.Hx, 75.30.Kz

I. INTRODUCTION

Following the discovery of superconductivity in Sr_2RuO_4 at ≈ 1 K[1] a wide interest in Ru-based perovskites has been generated, due to the diversity of the unusual physical properties discovered. Structurally related Ca_2RuO_4, which has the same crystal structure as the high-T_c superconductor $La_{2-x}Sr_xCuO_4$, is nonmetallic and shows an antiferromagnetic (AFM) ground state below $T_N = 110$ K.[2–4] On the other hand, $SrRuO_3$ and $CaRuO_3$ [$n = \infty$ members of the alkaline-earth-ruthenium Ruddlesden-Popper[5] series $(Sr, Ca)_{n+1}Ru_nO_{3n+1}$ are exceptionally interesting *per se*]. Both compounds adopt the same perovskite structure, with an orthorhombic distortion ($GdFeO_3$ structure type) and are metallic conductors. $SrRuO_3$ is the only known ferromagnetic (FM) conductor among the $4d$ oxides (the Curie temperature is $T_c = 165$ K), whereas $CaRuO_3$ was recently shown to have a spin-glass-like magnetic ground state.[6] Since a common structural feature of the two compounds is that they are composed of an array of corner-shared octahedra RuO_6, it is assumed that the degree of tilting and the rotation of these octahedra from an ideal cubic-perovskite structure governs the observed differences in the magnetic ground states. A narrow itinerant $4d$ band is formed through hybridization of Ru t_{2g} and O $2p$ orbitals. The $4d$ bandwidth thus formed sensitively depends on the degree of hybridization.[7] One of the powerful tools to study physical properties of such systems is realized through chemical substitution. Recent results on the effects of chemical substitutions in $CaRuO_3$ showed the following: $Ca_{0.95}Na_{0.05}RuO_3$ (Ref. 8) spin-glass or AFM ordering at 55 K, $CaRu_{1-x}Sn_xO_3$ (Ref. 9) spin-glass ordering for $4 \leqslant x \leqslant 10$ at. % Sn, a metal insulator transition (MIT) for $x \geqslant 16$ at. % Sn and $CaRu_{1-x}Rh_xO_3$ (Ref. 10) magnetic ordering (spin glass?) for all x, and a MIT for $x \geqslant 7$ at. % Rh. From these studies it is evident that the physical properties of $CaRuO_3$ are much more influenced by Rh than Sn substitution. Substitution of nonmagnetic Sn^{4+} for Ru^{4+} represents only lattice frustration and a magnetic dilution of a Ru sublattice. On the other hand, $Rh^{4+}(4d^5{:}t_{2g}^5e_g^0)$ with $S = \frac{1}{2}$, in the low-spin state, behaves as a magnetic impurity, since it substitutes $Ru^{4+}(4d^4{:}t_{2g}^4e_g^0)$ with a low spin $S = 1$. Nevertheless, it is likely that Rh assumes a valence state $Rh^{3+}(4d^6{:}t_{2g}^6e_g^0)$ $S = 0$ when incorporated into a Ru sublattice, and thus produces a charge frustration of the system. In order to clarify this issue, we have chosen $Cu^{2+}(3d^9)$, $S = \frac{1}{2}$, as a substitution for Ru^{4+}, since this inevitably represents both charge and spin frustration. $CaCuO_2$ is considered to be the parent of the cuprate family of superconducting compounds, consisting of CuO_2 sheets with an AFM ordering of Cu^{2+} neighboring cations. Although $CaRuO_3$ and $CaCuO_2$ are not isostructural, we have assumed that an appreciable amount of Cu can be incorporated into a Ru sublattice, while preserving the crystal structure. Furthermore, the recent discovery of the coexistence of magnetism and superconductivity in ruthenium-based layered cuprates $Ln_{1.4}Ce_{0.6}RuSr_2Cu_2O_{10-\delta}$ and $LnRuSr_2Cu_2O_8$ ($Ln = \text{Eu, Gd}$)[11–14] were an added motivation for this study.

In this paper we report results of magnetic and electrical resistivity properties of $CaRu_{1-x}Cu_xO_3$ ($0 \leqslant x \leqslant 15$ at. %Cu). We show here that Cu substitution on Ru sites profoundly alters the ground-state properties of $CaRuO_3$, introducing mixed oxidation states of Ru cations.

II. EXPERIMENTAL DETAILS

Polycrystalline samples of $CaRu_{1-x}Cu_xO_3$ ($0 \leqslant x \leqslant 15$ at. %Cu) were prepared by solid-state reaction from the appropriate stoichiometric mixtures of Ru metal powder, $CaCO_3$ and CuO (purchased from Strem Chemicals Inc.). The samples were mixed, ground, and preheated at 850 °C for 24 h in air. The powders were then reground, pressed into

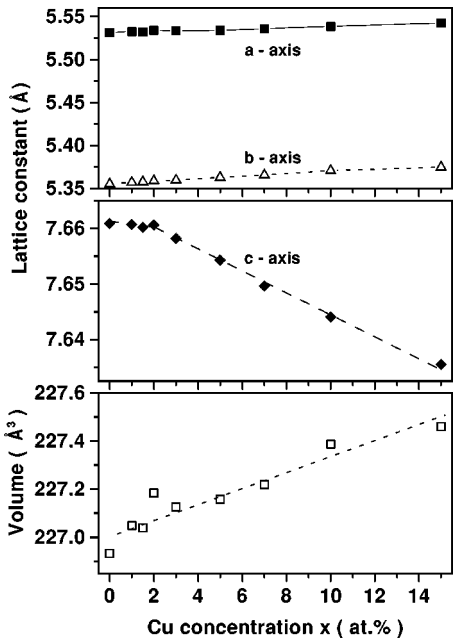

FIG. 1. Room-temperature lattice parameters and the volume of the unit cell vs the Cu concentration for polycrystalline $CaRu_{1-x}Cu_xO_3$.

pellets, and heated at 1000–1200 °C for 72 h in air, with two intermediate grindings. Single crystals of $CaRu_{1-x}Cu_xO_3$ ($x=0$, 5, 10, and 15 at. % Cu) were grown from a ground mixture of sintered samples and $CaCl_2$ flux in the ratio 1:30 (sample:flux). The mixture was heated to 1260 °C, and soaked at this temperature for 24 h, followed by slow cooling at a rate of 2 °C/h to 1000 °C, and finally quenched to room temperature to avoid possible twinning. The crystals tend to form in almost square planar shapes with sizes around $0.4\times0.4\times0.02$ mm^3, with short dimensions along the *c* axis. The single crystals and sintered polycrystalline samples were characterized by energy dispersive x-ray analysis and scanning electron microscopy and powder x-ray-diffraction (XRD) measurements. Powder x-ray-diffraction measurements were performed on a Philips 1010 powder diffractometer using Cu $K\alpha$ radiation at room temperature. dc magnetic measurements were performed by a Quantum Design superconducting quantum interference device magnetometer. Resistivity measurements were performed on polycrystalline samples employing a standard four-point method. Unfortunately, due to the extreme fragility of single crystals, several attempts to measure resistivity were not successful.

III. RESULTS AND DISCUSSION

The samples are of single phase, and crystallize in a perovskite structural type with an orthorhombic structure, space group *Pnma* (62). Our results for the lattice parameters of single-crystal and polycrystalline samples are in excellent agreement with values previously published.[15,16] At concentrations greater than 15-at. % Cu, small impurity diffraction lines of CuO appear, so that it is assumed that at this concentration the solubility limit is reached. The concentration dependence of the room-temperature lattice parameters and the volume of the unit cell for polycrystalline samples are shown in Fig. 1. The data for *a* and *b* axes show the expected Vegard's law linear expansion, assuming that larger Cu^{2+} (ionic radius 0.73 Å) substitutes for Ru^{4+} (the ionic radius is 0.62 Å). On the other hand, the *c* axis is almost constant below 2-at. % Cu, and then shows a linear shrinkage with increasing Cu concentration. A similar behavior was observed in $La_{2-x}Sr_xCu_{1-y}Ru_yO_{4-\delta}$ (Refs. 17 and 18) for $x=2$ and $0.7\leqslant y\leqslant1.0$. Nevertheless, the volume of the unit cell increases with *x*, as expected.

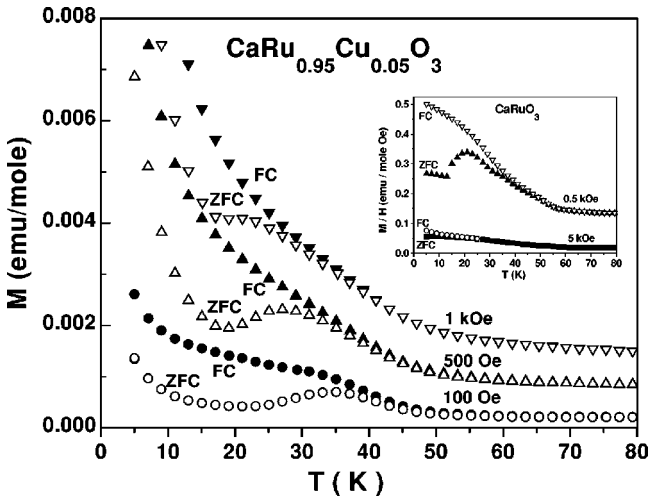

FIG. 2. $M(T)$ vs T (FC and ZFC) curves for a $CaRu_{0.95}Cu_{0.05}O_3$ single crystal measured at different magnetic fields applied along the *c* axis. Inset: $\chi(T)=M(T)/H$ vs T for a $CaRuO_3$ single crystal (H perpendicular to the *c* axis) (Ref. 6).

Shown in Fig. 2 is the magnetization vs temperature for a $CaRu_{0.95}Cu_{0.05}O_3$ single crystal measured at various values of magnetic field applied along the [001] direction, under field-cooled (FC) and zero-field-cooled (ZFC) conditions. An irreversibility phenomenon associated with the spin-glass-like behavior in $CaRuO_3$ (see the inset of Fig. 2) is clearly present in this case. Note the strong-field dependence of the irreversibility temperature T_{irr} (defined as the divergent point in the ZFC and FC curves). Furthermore, the broad peak around 35 K in the ZFC curve at 100 Oe is shifted to 29 K at 500 Oe, and completely smeared at 1 kOe.

The observed spin-glass behavior can be accounted for by assuming the following simple model: Cu^{2+} and/or Cu^{3+} substitution for Ru^{4+} produces a charge frustration of the system, and therefore requires a partial oxidation of neighboring Ru^{4+} cations to a higher valence state $Ru^{5+}(4d^3)$. This frustration is not local, since the next-to-nearest-neighbors will also be affected, undergoing a partial reduction to $Ru^{3+}(4d^5)$. In this manner, a charge compensation mechanism may affect the valence state and therefore the magnetic moment of Ru cations at appreciable distances from the Cu cation, simultaneously reducing the number of available conduction paths. According to Ref. 19, the signs of transfer integrals for 180° cation-anion-cation superexchange interactions between octahedral-site cations are predicted to be ferromagnetic for all $Cu^{2+/3+}$-$Ru^{3+/4+/5+}$ combinations and antiferromagnetic for Cu^{2+}-Cu^{2+}, Ru^{5+}-Ru^{3+}

(weak), Ru^{4+}-Ru^{3+} (weak), and Ru^{5+}-Ru^{5+} combinations. Therefore, mixed interactions, together with a random distribution of Cu atoms within a Ru sublattice, create the necessary ingredients for spin-glass ordering. Within the framework of the proposed scenario, ferromagnetic clusters are formed around Cu impurities with AFM interactions within and between clusters, introducing a frustration that results in a spin-glass behavior.

We fitted the data of $\chi(T)=M(T)/H$ (single crystal) in the paramagnetic range ($120\leqslant T\leqslant 250$ K) to the modified Curie-Weiss (CW) law $\chi(T)=\chi_0+C/(T-\theta)$, where χ_0 is the temperature-independent term, C is the Curie constant, and θ is the CW temperature. The value of the effective magnetic moment (deduced from the Curie constant C) $p_{\rm eff}=3.55\mu_B$ is remarkably close to the expected Hund's rule value $3.87\mu_B$ for Ru^{5+}, with $S=\frac{3}{2}$ and $g=2$, indicating the presence of Ru^{5+} in this mixed-valent system. This is in marked contrast to $p_{\rm eff}=2.33\mu_B$ obtained for a $CaRuO_3$ single crystal,[6] appropriate to the $2.83\mu_B$ expected for low-spin state ($S=1$) Ru^{4+}. The Curie-Weiss temperature θ also drastically changes from $-36(1)$ K for $CaRuO_3$ to $-134(3)$ K for $CaRu_{0.95}Cu_{0.05}O_3$, showing enhanced AFM interactions. Furthermore, a measure of the density of states near the Fermi surface drops from $\chi_0=9.5\times10^{-3}$ emu/mole Oe at $x=0$ to $\chi_0=7\times10^{-4}$ emu/mole Oe at $x=0.05$. This is consistent with the resistivity behavior measured on polycrystalline samples shown in Fig. 7, where the onset of a MIT is observed at 51 and 69 K for $x=0.02$ and 0.05 Cu concentrations, respectively.

Although these results support the charge compensation mechanism outlined above, still another possibility for charge compensation realized by oxygen loss, i.e., the creation of oxygen vacancies, can be significant. It was shown for $La_{2-x}Sr_xCu_{1-y}Ru_yO_{4-\delta}$,[18] with a K_2NiF_4-type structure, that the oxygen vacancies are located exclusively in the vicinity of Cu cations, which consequently means a local character of the charge compensation. However, thermogravimetric analysis results showed a decrease of the oxygen content with increasing Cu concentration for $x>7$ at. % Cu, which is consistent with electrical resistivity measurements. That is, the lower concentration of Ru^{5+}, due to the presence of oxygen vacancies, should increase conductivity and shift the MIT to higher Cu concentrations, simultaneously reducing the MIT temperature for fixed x. Indeed, resistivity measurements (not shown here) performed on slightly reduced polycrystalline samples (annealed at 350 °C in a N_2 atmosphere for 1 h) showed a metallic behavior in the measured temperature range $7\leqslant T\leqslant 300$ K for $x\leqslant 3$ at. % Cu, and a decrease of the MIT temperature from 87 to 30 K for $x=7$ at. % Cu.

Magnetic isotherms $M(H)$ at $T=5$ K, obtained after cooling in zero applied field for an almost square planar-shaped $CaRu_{0.95}Cu_{0.05}O_3$ single crystal and polycrystalline samples, are shown in Fig. 3. With an increasing applied field along the c axis, $M(H)$ reaches saturation for $H\geqslant 2$ T, yielding very low saturation moment $p_0=0.044\mu_B$. On the other hand, $M(H)$ for a field applied perpendicular to the c axis (i.e., in-plane), shows no sign of saturation up to

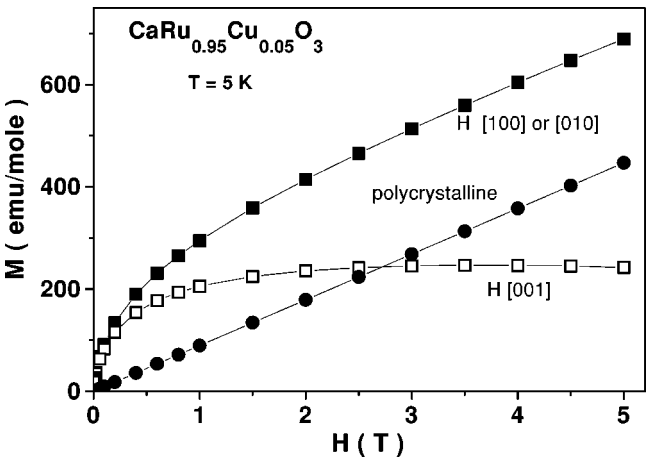

FIG. 3. Magnetic isotherms at $T=5$ K for $x=5$ at. % Cu single-crystal and polycrystalline materials.

$H=5$ T. This behavior is markedly different from the anisotropy of the magnetization found in single-crystal $CaRuO_3$,[6] where an easy axis of magnetization along the c axis is determined. The isothermal magnetization obtained for a polycrystalline $CaRu_{0.95}Cu_{0.05}O_3$ sample shows a linear behavior, with no qualitative difference from that obtained for polycrystalline $CaRuO_3$. Small hysteresis loops at $T=5$ K (not shown here), with essentially the same coercive field of $H_c\approx 100$ Oe for both polycrystalline and single crystal samples, are observed.

The temperature dependence of the magnetic susceptibility for polycrystalline $CaRu_{0.9}Cu_{0.1}O_3$ (a) and $M(T)$ for single-crystal (b) $CaRu_{0.9}Cu_{0.1}O_3$ are shown in Fig. 4. Apart from the different irreversibility temperatures $T_{\rm irr}$, observed for polycrystalline and single-crystal materials (also present for $x=0$ and 5 at. % Cu), a truly remarkable difference is manifested here both in the shapes of the FC and ZFC curves and the onset of magnetic ordering at T_0 for polycrystalline samples, but without any magnetic anomaly present in single crystals in this temperature range. $\chi(T)$ data for the polycrystalline $CaRu_{0.9}Cu_{0.1}O_3$ sample show $T_{\rm irr}\approx 80$ K and a well-defined maximum in the ZFC curve at $T_0\approx 9.2$ K ($H=14$ Oe) [Fig. 4(a)]. At $H=1$ kOe, $T_{\rm irr}$ is completely suppressed, being essentially equal to T_0, which is slightly shifted to lower temperatures at this field. On the other hand, $M(T)$ data for single-crystal $CaRu_{0.9}Cu_{0.1}O_3$ resemble reentrant spin-glass behavior. Note the pronounced FM-like shape of FC curves, and also the difference between $T_{\rm irr}$ and the onset of FM-like behavior. $T_{\rm irr}$ is strongly field dependent, decreasing rapidly with increasing field.

The increase of Cu concentration promotes the growth of FM clusters, tending to establish long-range FM order. However, this process is opposed by two effects: (1) The influence of short range AFM interactions within and between FM clusters may become more prominent in sintered polycrystalline samples with randomly oriented microcrystallites than in macroscopic single crystals, thereby leading to a freezing of magnetic moments at low temperatures. Spin disorder at grain boundaries and surfaces was extensively studied recently,[20–23] including the size-dependent magnetic

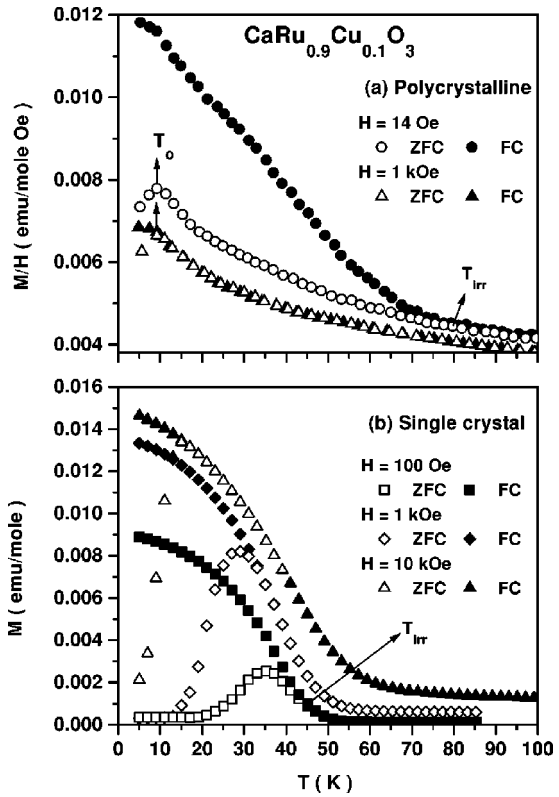

FIG. 4. FC and ZFC curves for $CaRu_{0.9}Cu_{0.1}O_3$ at different magnetic fields: (a) $\chi(T)$ vs T for polycrystalline sample, and (b) $M(T)$ vs T for single crystal (H perpendicular to the c axis).

properties.[24] We believe that these effects are present in this case, especially because the material shows intrinsic spin-glass properties. (2) The decrease of the average distance between Cu cations with increasing concentrations leads to increased concentrations of Ru^{5+} cations and thus a higher probability for Ru^{5+}-Ru^{5+} AFM superexchange interactions. The formation of Cu-O-Cu pairs, triplets, etc., and the creation of oxygen vacancies at higher Cu concentrations add to the complexity of the magnetic properties. The former effect provides a possible explanation for differences in the magnetic properties between polycrystalline and single-crystal $CaRu_{0.9}Cu_{0.1}O_3$. The growth of FM clusters is almost unrestricted in single crystals, which is reflected in the extremely large coercive field $H_c = 2.2$ T [see Fig. 5(a)]. The saturation moment $p_0 = 0.14\mu_B$ deduced from the $M(H)$ curve is significantly higher than $p_0 = 0.044\mu_B$ obtained for $CaRu_{0.95}Cu_{0.05}O_3$. The extracted paramagnetic values in the range $120 \leqslant T \leqslant 250$ K are $\chi_0 = 3.6 \times 10^{-4}$ emu/mole Oe, $\theta = -219$ K, and $p_{\text{eff}} = 3.48\mu_B$. The increase of the Cu concentration from 5- to 10-at.% Cu also leads to profound changes in the $\rho(T)$ behavior (see Fig. 7), showing a sharp increase of the MIT temperature from 87 K to above 300 K for $x = 7$ and 10 at.% Cu, respectively.

Shown in Fig. 6 are the magnetic susceptibility $\chi(T)$ vs the temperature dependence for a polycrystalline (a) $CaRu_{0.85}Cu_{0.15}O_3$ sample, and $M(T)$ for a single-crystal (b) $CaRu_{0.85}Cu_{0.15}O_3$ samples. Both effects mentioned above should be considered in this case, since the low-temperature magnetic anomaly at T_0, associated with a freezing of FM

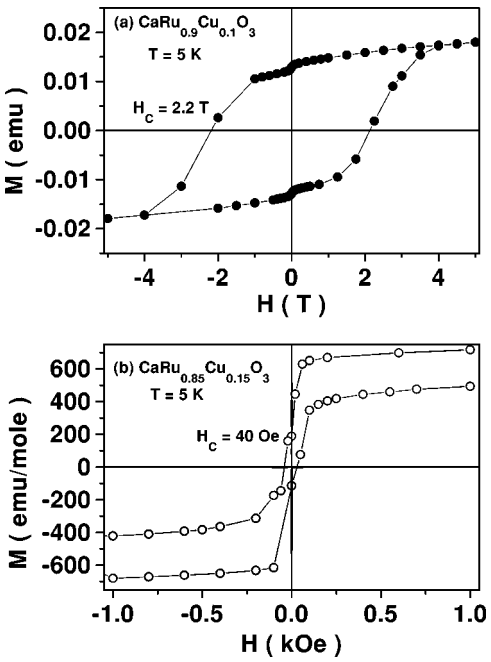

FIG. 5. Magnetic hysteresis loops at $T = 5$ K (ZFC) for single crystals: (a) $CaRu_{0.9}Cu_{0.1}O_3$ and (b) $CaRu_{0.85}Cu_{0.15}O_3$. The field is applied perpendicular to the c axis in both cases.

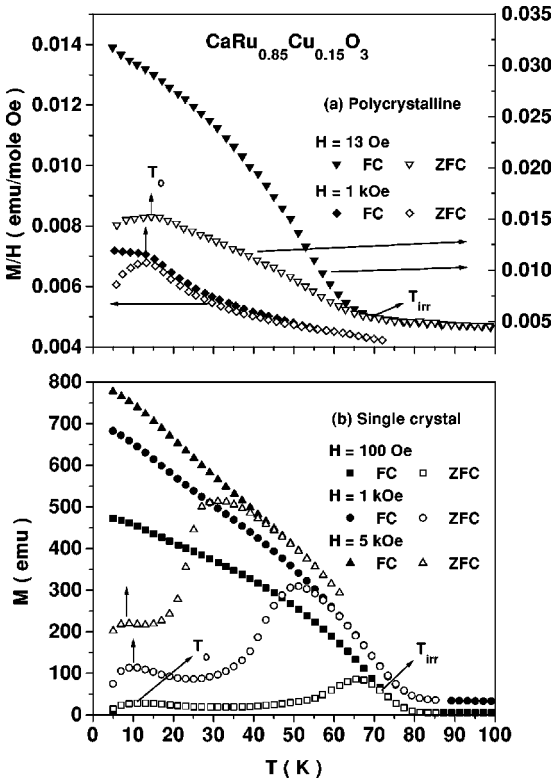

FIG. 6. FC and ZFC curves for $CaRu_{0.85}Cu_{0.15}O_3$ measured at different magnetic fields: (a) $\chi(T)$ vs T for a polycrystalline sample, and (b) $M(T)$ vs T for a single crystal (H perpendicular to the c axis).

clusters, is present in polycrystalline and single-crystal materials. However, note the change of shape of the FC curve for a polycrystalline sample at $H=1$ kOe, and also the change of slope at T_0, which are not seen in single crystals. The onset of a FM-like behavior at 70–80 K (FC curves) is very close for both forms of material, and is virtually field independent for single crystals. Moreover, $T_{\rm irr}$ is also approximately equal, and decreases rapidly with increasing field in a similar manner. The behavior of the low-temperature magnetic anomaly observed in ZFC curves vs magnetic field is very similar for both single-crystal and polycrystalline samples, and shows a slight temperature decrease with increasing field, being completely washed out at $H>7.5$ kOe in single crystals.

The magnetic hysteresis loop measured on single crystals after zero-field cooling [see Fig. 5(b)] is drastically smaller, $H_c=40$ Oe, than that seen for $x=10$ at. % Cu, while the saturation moment $p_0=0.2\mu_B$ is somewhat larger, in accordance with differences in magnetic properties. Fitting $\chi(T)$ to the CW law within the $120\leqslant T\leqslant 250$ K range yields $\theta=-33.9$ K, $p_{\rm eff}=2.24\mu_B$, and $\chi_0=4.8\times10^{-3}$ emu/mole Oe. The higher Cu concentration, the inevitable presence of oxygen vacancies at these concentrations, and the temperature range of fitting (the vicinity of the magnetic transition at $\approx$80 K) may account for the striking change of the extracted paramagnetic values compared with those obtained for $x=5$ and 10 at. % Cu single crystals.

Shown in Fig. 7 are the electrical resistivity data vs temperature for polycrystalline $CaRu_{1-x}Cu_xO_3$ samples. Although there is a close temperature correspondence between changes of slope of $d(\ln\rho)/d(T^{-1/4})$ vs $T^{-1/4}$ and $T_{\rm irr}(T_0)$ for low applied magnetic-field $M(T)$ data (polycrystalline samples), the plots for $\ln\rho$ vs temperature to the $-\nu$th power $(\frac{1}{4}\leqslant\nu\leqslant1)$ do not show linear parts in any temperature regions for any ν values. Therefore, formulas for the variable-range-hopping resistivity do not match exactly with the resistivity data. This is not surprising, considering the large differences in magnetic properties between single-crystal and polycrystalline samples due to grain boundaries.

More detailed research, employing a precise control of the oxygen stoichiometry and complementary experimental methods, could provide the basis for a full characterization of the $CaRu_{1-x}Cu_xO_3$ system. However, the main result of this study shows that substitution of a $Cu^{2+/3+}$ cation for Ru^{4+} changes the valence state of the latter to Ru^{5+}, thereby introducing drastic changes in both the resistivity and magnetic properties of the parent compound. Keeping in mind the obvious differences, the similarity in $\rho(T)$ and $\chi(T)$ behaviors with $CaRu_{1-x}Rh_xO_3$ (Ref. 10) is quite appealing. While the spin-glass-like behavior in $CaRu_{1-x}Cu_xO_3$ (for $x>0$) can be understood, at least qualitatively, the origin of the spin-glass-like transition observed in pure $CaRuO_3$ (lacking an evident source of perturbation) must be more subtle in nature, and is *not related* to the former. Therefore, we conclude that chemical probes, which potentially alter the valence state of Ru^{4+} in (Ca, Sr)RuO_3, are not adequate tools for obtaining deeper insight into physical properties of the parent compound. In this sense a nonmagnetic probe like Sn^{4+} can provide much more information. A discussion of this issue is beyond the scope of this paper, and will be published elsewhere.

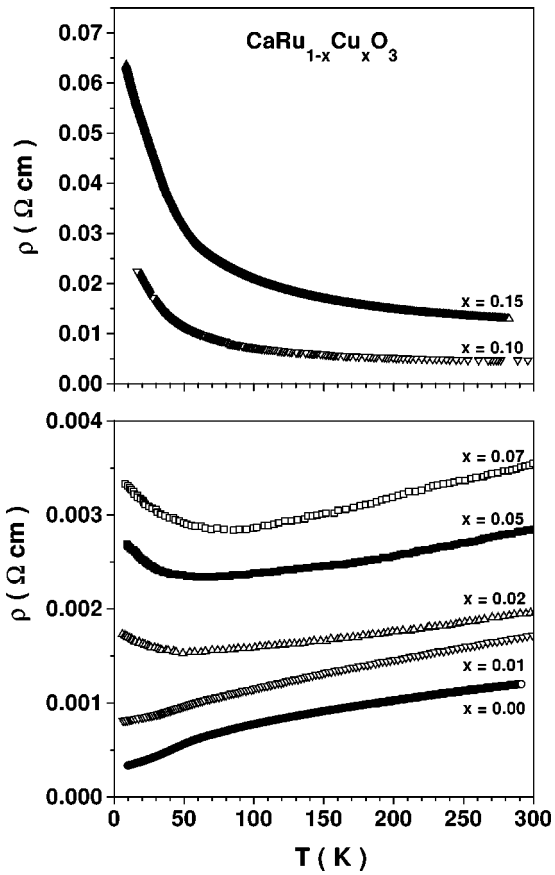

FIG. 7. Electrical resistivity $\rho(T)$ vs temperature T for polycrystalline $CaRu_{1-x}Cu_xO_3$ samples.

IV. CONCLUSIONS

In summary, we have shown that substitution of $Cu^{2+/3+}$ for Ru^{4+} in $CaRu_{1-x}Cu_xO_3$ alters the oxidation state of the neighboring Ru cations to Ru^{5+}, leading to a spin-glass-like behavior for lower Cu concentrations ($x\leqslant7$ at. % Cu), and to complex magnetic behaviors for $x\geqslant10$ at. % Cu. Simultaneously, the MIT is observed for only 2-at. % Cu at 51 K. The physical processes involved, while being interesting *per se* and possibly useful for understanding complexities of other materials like $GdRuSr_2Cu_2O_8$,[14] have different origins and therefore cannot be related to the physical properties of the parent compound $CaRuO_3$.

ACKNOWLEDGMENTS

We are indebted to Dr. D. Rodić for help in the XRD analysis. I. M. B. gratefully acknowledges support from the ''Abdus Salam'' ICTP, Trieste, Italy. The work in Jerusalem was supported by the BSF (1999).

*Corresponding author. Fax: +381 11 3440 100, e-mail: bradaric@rt270.vin.bg.ac.yu

[1] Y. Maeno, H. Hashimoto, K. Yoshida, S. Nishizaki, T. Fujita, J. G. Bednorz, and F. Lichtenberg, Nature (London) **372**, 532 (1994).
[2] S. Nakatsuji, S. Ikeda, and Y. Maeno, J. Phys. Soc. Jpn. **66**, 1868 (1997).
[3] G. Cao, S. McCall, M. Shepard, J. E. Crow, and R. P. Guertin, Phys. Rev. B **56**, R2916 (1997).
[4] M. Braden, G. Andre, S. Nakatsuji, and Y. Maeno, Phys. Rev. B **58**, 847 (1998).
[5] S. N. Ruddlesden and P. Popper, Acta Crystallogr. **11**, 54 (1958).
[6] I. Felner, I. Nowik, I. Bradarić, and M. Gospodinov, Phys. Rev. B **62**, 11 332 (2000).
[7] P. A. Cox, R. G. Egdell, J. B. Goodenough, A. A. Hamnett, and C. C. Naish, J. Phys. C **16**, 6221 (1983).
[8] M. Shepard, G. Cao, S. McCall, F. Freibert, and J. E. Crow, J. Appl. Phys. **79**, 4821 (1996).
[9] G. Cao, S. McCall, J. Bolivar, M. Shepard, F. Freibert, P. Henning, J. E. Crow, and T. Yuen, Phys. Rev. B **54**, 15 144 (1996).
[10] G. Cao, F. Freibert, and J. E. Crow, J. Appl. Phys. **81**, 3884 (1997).
[11] L. Bauernfeind, W. Widder, and H. F. Braun, Physica C **254**, 151 (1995).
[12] L. Bauernfeind, W. Widder, and H. F. Braun, J. Low Temp. Phys. **105**, 1605 (1996).
[13] I. Felner, U. Asaf, Y. Levi, and O. Millo, Phys. Rev. B **55**, R3374 (1997).
[14] J. W. Lynn, B. Keimer, C. Ulrich, C. Bernhard and J. L. Tallon, cond-mat/0001456 31 (unpublished); Phys. Rev. B **61**, R14 964 (2000).
[15] H. Kobayashi, M. Nagata, R. Kanno, and Y. Kawamoto, Mater. Res. Bull. **29**, 1271 (1994).
[16] G. Cao, S. McCall, M. Shepard, and J. E. Crow, Phys. Rev. B **56**, 321 (1997).
[17] S. Ebbinghaus and A. Reller, Solid State Ionics **101–103**, 1369 (1997).
[18] S. Ebbinghaus, M. Fröba, and A. Reller, J. Phys. Chem. B **101**, 9909 (1997).
[19] J. B. Goodenough, in *Magnetism and the Chemical Bond*, (Wiley, New York, 1966), p. 174.
[20] N. Zhang, S. Zhang, W. P. Ding, W. Zhong, and Y. W. Du, Solid State Commun. **107**, 417 (1998).
[21] N. D. Mathur, G. Burnell, S. P. Isaac, T. J. Jackson, B.-S. Teo, J. L. MacManus-Driscoll, L. F. Cohen, J. E. Evetts, and M. G. Blamire, Nature (London) **387**, 266 (1997).
[22] R. H. Kodama, A. E. Berkowitz, E. J. McNiff, Jr., and S. Foner, Phys. Rev. Lett. **77**, 394 (1996).
[23] B. Martinez, X. Obradors, Ll. Balcells, A. Rouanet, and C. Monty, Phys. Rev. Lett. **80**, 181 (1998).
[24] J. P. Chen, C. M. Sorensen, K. J. Klabunde, G. C. Hadjipanayis, E. Devlin, and A. Kostikas, Phys. Rev. B **54**, 9288 (1996).